Plastic Flow and Fracture of Metallic Glass

H. J. LEAMY, H. S. CHEN, AND T. T. WANG

The tensile flow and fracture behavior of three $Pd_{0.8}Si_{0.2}$-based alloys in the glassy, "microcrystalline," and fully crystalline condition has been studied. The glassy alloys flow plastically to a total strain of approximately 0.5 pct ϵ, and exhibit proportional limit stresses of approximately $E \times 10^{-2}$ where E is Young's modulus. This plastic flow is accompanied by the formation of shear deformation bands on the specimen surfaces. Fully crystalline alloys are extremely brittle and fracture via intergranular cracking. Fracture surfaces of the amorphous and "microcrystalline" alloys are inclined at 45 deg to the tensile axis and exhibit two morphologically distinct zones. One zone is relatively featureless while the other contains a "river" pattern of local necking protrusions. Detailed comparison of opposing surfaces indicates that fracture is preceded by large local plastic shear which produces the smooth zone while the local necking pattern is produced during rupture. These observations form the basis for the hypothesis that plastic flow in the glassy material occurs via localized strain concentrations and that fracture is initiated by catastrophic, "adiabatic" shear.

THE formation of the amorphous state in metallic materials by quenching from the liquid was first reported in 1960.[1] Subsequently, several glass forming, metallic alloys have been discovered and studied, usually with a view towards elucidation of the glass-liquid transition or glassy structure. Among these, perhaps the most well characterized are alloys based on $Pd_{0.8}Si_{0.2}$, whose thermal,[2] electrical,[3] structural,[4] and mechanical[5-7] properties have been investigated. In the glassy state, these alloys are reported to possess a structure[8] which closely approximates Bernal's[9] dense random packing model for a monatomic liquid. That is, they are structurally simpler than inorganic or polymer glasses and are therefore ideal subjects for testing theories of the glassy state. The phenomena of plastic or "cold" flow and fracture in these materials is of particular interest, since structural considerations are of paramount importance in these processes. In this paper we present experimental observations of the external manifestations of flow and fracture produced by indentation, bending, and tension in three $Pd_{0.8}Si_{0.2}$-based alloys in the glassy, microcrystalline, and crystalline states.

EXPERIMENTAL METHODS

Specimens for this study were produced by dropping a molten alloy charge between a pair of rapidly rotating steel rollers.[10] Uniform strips 40 to 100 μ thick and 3 to 5 mm wide were formed by solidification of the alloy during its contact with the rollers. These were cut into 3 by 30 mm ribbons, vacuum encapsulated in quartz ampoules, heat treated, and examined by X-ray diffraction prior to testing. Tensile tests were carried out at room temperature and at a strain rate of 1.1×10^{-3} sec^{-1}. Following deformation, the specimens were examined with a JSM-U3* scanning electron microscope operating at 25 kv in the secondary electron emission mode. The compositions, structures, and glass transition and crystallization temperatures[2] of the alloys examined in this investigation are summarized in Table I. The gold and copper alloying additions shown in Table I were selected because they increase the stability and glass transition temperature of the binary alloy, presumably by increasing the configurational entropy and hence the stability of the liquid phase.[2] This effect is evidenced by an increase in the crystallization temperature, T_c, as shown in Table I.

The amorphous-crystalline transformation in these alloys has been studied previously. For the binary alloy,[2] crystallization occurs in three stages: a) homogeneous precipitation of a very fine-grained, "microcrystalline" (20 to 100Å) metastable fcc phase within

*Japan Electron Optics Laboratory Co., Ltd., Medford, Mass.

H. J. LEAMY and T. T. WANG are Members of the Technical Staff, Bell Telephone Laboratories, Inc., Murray Hill, N. J. H. S. CHEN, formerly Postdoctoral Associate, Yeshiva University, New York, N. Y., is now Staff Physicist, Allied Chemical Corp., Materials Research Center, Morristown, N. J.

Manuscript submitted August 4, 1971.

Table I. Pd-Si Specimen Compositions, Heat Treatments, Structures, and Transformation Temperatures

No.	Composition, Atomic Fractions	Heat Treatment	Structure	T_g*	T_c*
1	$Pd_{0.82}Si_{0.18}$	as quenched	amorphous	362°C	367°C
2	$Pd_{0.82}Si_{0.18}$	350°C/18 hr furnace cool	glass microcrystalline fcc + metastable silicide		
3	$Pd_{0.82}Si_{0.18}$	450°C/2 hr furnace cool	fcc + metastable silicide		
4	$Pd_{0.795}Au_{0.04}Si_{0.165}$	as quenched	amorphous	372°C	402°C
5	$Pd_{0.795}Au_{0.04}Si_{0.165}$	350°C/18 hr.	glass + fcc microcrystals		
6	$Pd_{0.795}Au_{0.04}Si_{0.165}$	450°C/2 hr. furnace cool	microcrystalline fcc + metastable silicide		
7	$Pd_{0.775}Cu_{0.06}Si_{0.165}$	as quenched	amorphous	373°C	413°C
8	$Pd_{0.775}Cu_{0.06}Si_{0.165}$	350°C/18 hr furnace cool	glass + microcrystalline fcc		
9	$Pd_{0.775}Cu_{0.06}Si_{0.165}$	450°C/2 hr furnace cool	glass + microcrystalline fcc + metastable silicide		

*T_g and T_c values from Ref. 2. Heating rate = 20°C per min.

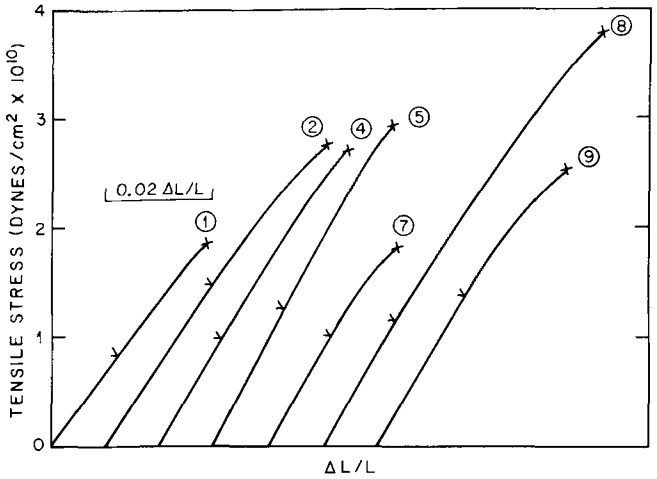

Fig. 1—Load-elongation curves for the tensile specimens listed in Table I.

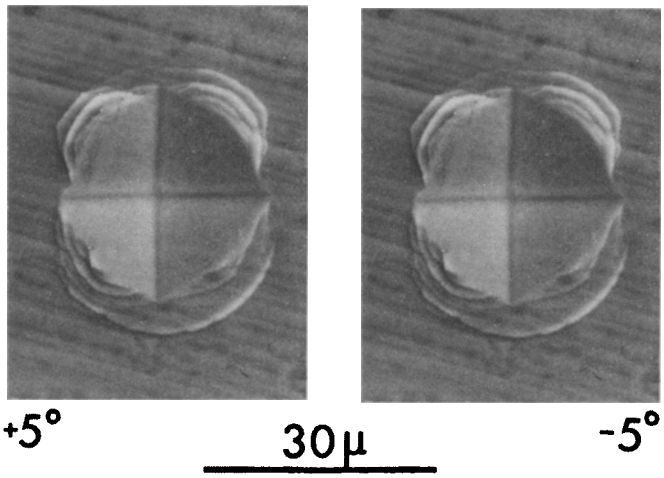

Fig. 2—Stereo pair of micrographs of a 50 g dph indentation in an amorphous $Pd_{0.82}Si_{0.18}$ alloy. The tilt axis is vertical and rotation is taken as positive in the clockwise direction.

Table II. Mechanical Properties of PdSi Alloys

Number	DPH, kg/mm²	*E*, dyne/cm²	YS, dyne/cm²	UTS, dyne/cm²	TS	YS/E
1	118	6.8×10^{11}	8.25×10^{9}	2.7×10^{10}	0.0025	1.21×10^{-2}
2	116	7.5×10^{11}	1.35×10^{10}	2.75×10^{10}	0.004	1.5×10^{-2}
3	232	Specimens extremely brittle no tensile data		0		
4	127	8.5×10^{11}	9.5×10^{9}	2.7×10^{10}	0.003	1.12×10^{-2}
5	91	10×10^{11}	1.25×10^{10}	2.95×10^{10}	0.003+	1.25×10^{-2}
6	161	Specimens extremely brittle no tensile data		0		
7	129	8.25×10^{11}	1.0×10^{10}	1.82×10^{10}	0.003	1.11×10^{-2}
8	113	9.0×10^{11}	1.15×10^{10}	3.55×10^{10}	0.009	1.40×10^{-2}
9	141	9.0×10^{11}	1.37×10^{10}	2.52×10^{10}	0.004	1.89×10^{-2}

Notes: DPH = diamond pyramid hardness, average of 4 values; *E* = Young's modulus; YS = Yield stress; UTS = Ultimate tensile stress; and TS = Plastic strain at fracture.

the glassy matrix, b) precipitation of a metastable silicide of unknown structure, and c) precipitation of the equilibrium Pd + Pd_3Si phases. As noted in Table I, binary alloys annealed at 350° and 450°C possess structures corresponding to stages (a) and (b) above, respectively. Crystallization of the ternary alloys proceeds along a similar course but is further complicated by phase separation in the glassy state at annealing temperatures near 450°C. This phase separation is not detectable by the X-ray methods used to characterize the alloy structures in this study, but is presumed to occur on the basis of previous transmission electron microscopy experiments.[2]

RESULTS

a) Tensile Properties

Tensile load-elongation curves for the alloys listed in Table I are shown in Fig. 1. In every instance, these curves are characterized by the absence of a well-defined plastic yield and a high apparent hardening rate. The yield stress data shown in Table II were therefore taken equal to the proportional limit. For the binary alloy, good agreement with the recently reported results of Masumoto and Maddin[7] was obtained. In addition, the Young's modulus of the gold containing alloy agrees well with that determined by dynamic methods.[6] In every case, the modulus of the amorphous alloy is smaller than that of its microcrystalline counterpart. This behavior has been noted previously[6,11] and Weaire *et al.*[12] have attributed it to the internal atomic displacements which accompany shear deformation. Note that the modulus, yield stress, ultimate strength, and strain at fracture of the crystalline specimens are higher than the amorphous alloys. Both flow and fracture are evidently initiated more easily in the glassy than in the microcrystalline state.

b) Hardness Measurement

The diamond pyramid hardness numbers of the alloys are also given in Table II. For the values of *YS/E* encountered here, the hardness indenter may be treated as a flat die penetrating an elastic-plastic material. In this case, we expect plastic flow to produce an extrusion lip at the edge of the indentation.[13] That this is indeed the case is illustrated in Fig. 2, where a stereo pair of micrographs of a 50 g indentation in specimen No. 1 is shown.* The plastic deformation evident in this figure cannot be attributed to the densification processes which occur in some oxide glasses,[14] because the density of the glassy phase differs insignificantly from that of the crystalline phase. All of the alloys listed in Table I exhibited a similar indentation morphology.

*This and subsequent scanning electron micrographs are oriented such that the scanning direction is horizontal from left to right. The secondary electron detector is located to the right of the scanned area.

c) Tensile Fracture Morphology

Fig. 3 shows the fracture surfaces of opposing segments of a typical, unannealed amorphous specimen. This specimen (alloy No. 4) fractured on two macroscopic surfaces, each oriented approximately 45 deg from the tensile axis. The region of transition from one to the other of these is shown in the left portion of Fig. 3, and in greater detail on the right. Although the stress-strain curves for the amorphous alloys show

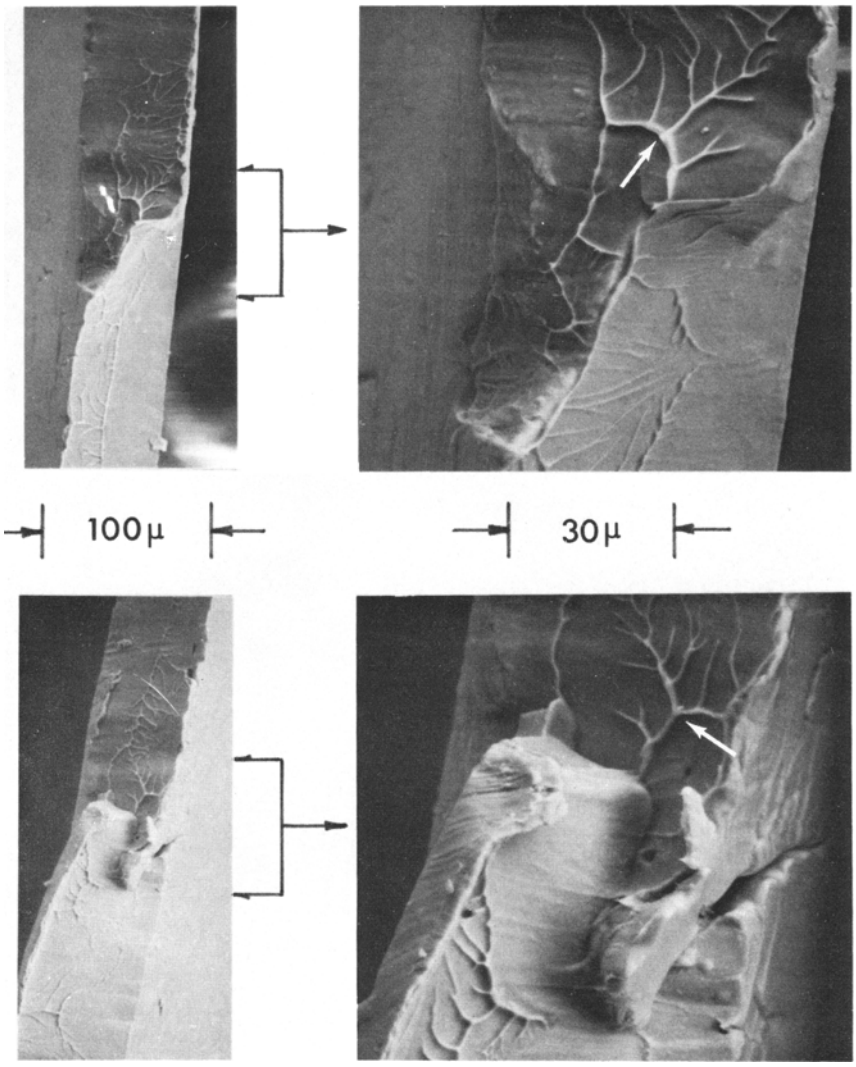

Fig. 3—The tensile fracture morphology of an unannealed amorphous, $Pd_{0.795}Au_{0.04}Si_{0.165}$ alloy (tensile specimen No. 4). The surfaces of opposing segments of the fractured specimens are shown in the upper and lower pairs of micrographs. The white arrows mark corresponding points on the two surfaces.

little ductility, it is apparent that this material does not fracture in a typical glassy or brittle manner; *i.e.* the two complementary fracture surfaces are not mirror images on a microscopic scale and the fracture surfaces are not normal to the tensile axis. Stereomicroscopy experiments confirm that the "vein" structures apparent in Fig. 3 are *protrusions* on *both* fracture surfaces. Furthermore, the patterns formed by these protrusions on opposing fracture surfaces are similar but not identical. The arrows in Fig. 3 mark corresponding points on the opposing surfaces. We take these observations as evidence for the occurrence of local necking during the fracture of this metallic glass.

In areas removed from the transition region shown in Fig. 3, the fracture morphology consists of two easily distinguished zones, as shown in Fig. 4. The zone located uppermost in the top micrograph of Fig. 4 is characterized by its lack of a local necking pattern and generally smooth appearance. This zone gives way abruptly to a region in which local necking is evident. Note that the "veins" and the regions between them are quite smooth, and that they form a pattern reminiscent of the "river" patterns formed during cleavage fracture of brittle crystalline material.[15] On this basis, the point of crack initiation is evidently near the center of the intermediate magnification micrograph in Fig. 4, *i.e.*, at the smooth region where the "vein" patterns converge. Long, necked filaments are commonly observed at triple point junctions of local necking ridges, as shown in Fig. 5. These filaments, often nearly 1 μ long, are usually elongated in the tensile direction but occasionally, as in Fig. 5, appear to have relaxed into a curved position. In every case, the tips of the filaments are rounded, as if by viscous flow. Fig. 5, which was obtained from a microcrystalline specimen (No. 5) also shows that the regions between local necking ridges are rougher than corresponding regions on the glassy alloy fracture surfaces. This is the single significant difference between the amorphous and microcrystalline alloy fracture morphologies.

In contrast to the amorphous and microcrystalline specimens, those containing large amounts of metastable silicide were extremely brittle and invariably fractured during handling. One such fracture is shown in Fig. 6. The fracture consists of two zones. The region of crack initiation is quite rough, the fracture being apparently intergranular in this region, while the remaining zone is rough on a much finer scale.

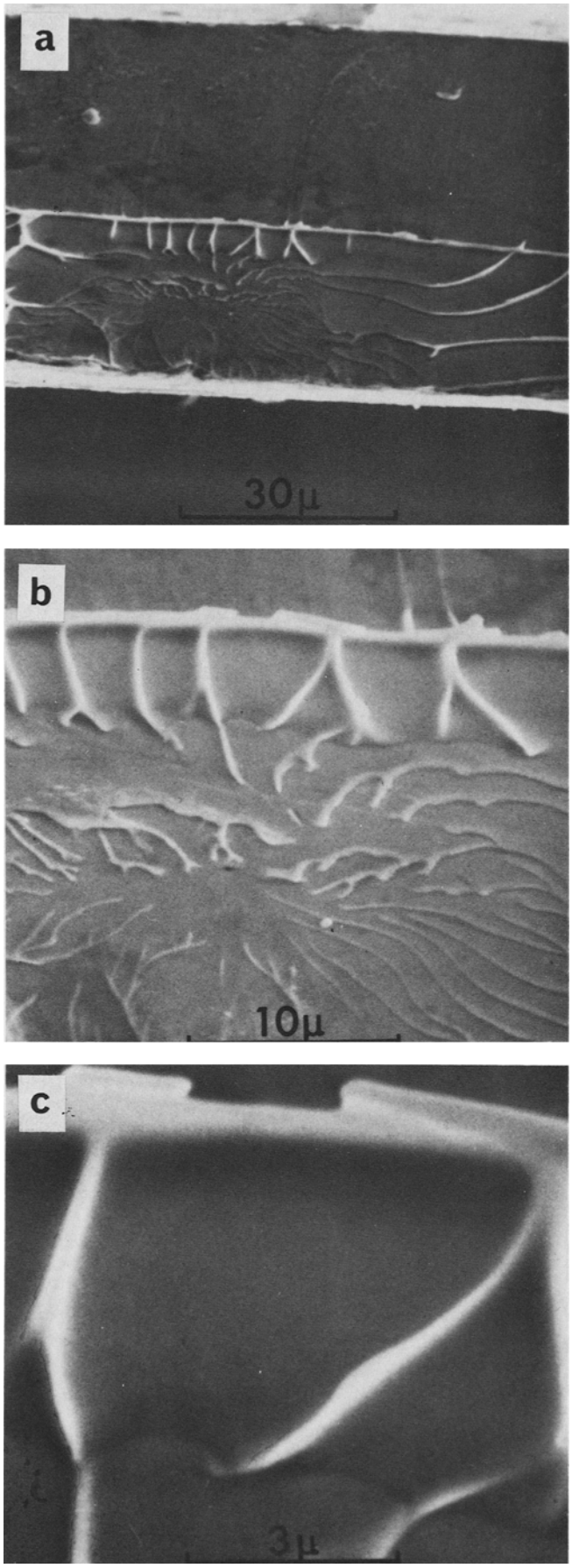

Fig. 4—A typical two zone tensile fracture in an amorphous $Pd_{0.795}Au_{0.04}Si_{0.165}$ alloy (tensile specimen No. 4).

The features present in Figs. 3 and 4 are common to *all* of the amorphous *and* microcrystalline alloy fracture surfaces and may be summarized as follows:

a) Fracture occurs on surfaces whose normals lie at 45 ± 2 deg to the tensile axis in the plane of the tensile axis and the ribbon surface normal. That is, fracture occurs on planes of maximum shear stress.

b) Fracture invariably involved one and occasionally two transitions from one to the other plane of maximum shear stress.

c) Two distinct fracture zones are present: a nearly smooth region, and one in which local necking "vein" patterns are observed. The "veins" are the order of 0.1 μ in width and generally possess a height-to-width ratio of from two to four, except at triple point junctions where micron-length necked filaments are often observed.

The shear nature of the deformation process described above was confirmed by bend test experiments. The deformation markings on the tensile stress side of ribbon specimens bent to various radii of curvature are shown in Fig. 7. At large radii, bending produces long straight plastic shear deformation steps parallel to the bend axis. Further bending leads to production of secondary steps at small angles to the primary steps and finally to large shear displacements at these steps. The absence of tensile cracks is particularly to be noted in Fig. 7.

The remarkable shear failure of these specimens may be envisioned as propagating in several possible modes. These are illustrated schematically in Fig. 8. In the first case, Fig. 8(*a*), a shear crack propagates from the surface through a portion of the specimen and creates the smooth fracture zone. At the now increased stress levels, shear cracks (voids) in the remaining sound material may link together during fracture to produce the observed vein structure. Alternatively, Fig. 8(*b*), the specimen may undergo plastic shear deformation and subsequently fail by propagation and linking of internal shear cracks or voids. Finally, the alternating shear mechanism proposed by Pelloux[16] to account for observations of shear failure[17,18] in steels tested near their ductile-brittle transition temperature is shown in Fig. 8(*c*).

Of these mechanisms, only those shown in Figs. 8(*a*) and 8(*b*) produce fracture surfaces which possess the characteristics observed in this study. These mechanisms may be distinguished by comparison of the morphology of opposing fracture surfaces. Such a comparison is shown in Fig. 9. The micrographs in the left-hand column of Fig. 9 were obtained from one segment of specimen No. 1 while those on the right were obtained from the corresponding area on the opposite segment. The left-hand column of micrographs was printed with the negative reversed to allow direct comparison of the vein patterns. The area selected for Fig. 9 contains an easily recognized vein pattern which is observed to be nearly identical on each fracture surface. The *position* of this pattern on the left set of micrographs is displaced significantly with respect to its position on the other fracture surface. This provides clear evidence for the failure mode shown in Fig. 8(*b*) and leads to the conclusion that plastic shear deformation of as much as 40 pct precedes failure in these specimens. However, the high apparent hardening rate shown in Fig. 1 should lead

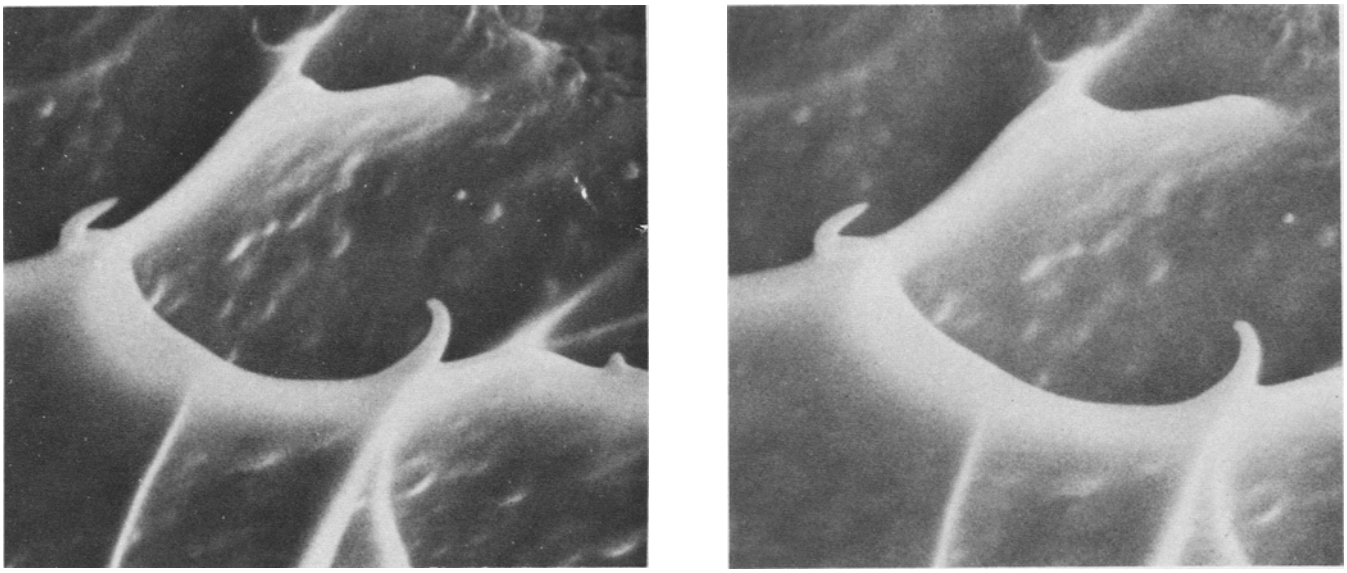

Fig. 5—Stereo pair of micrographs illustrating extensive local necking at triple point junctions in a microcrystalline $Pd_{0.795}Au_{0.04}Si_{0.165}$ alloy (tensile specimen No. 5).

to a homogeneous distribution of plastic strain while the displacement shown in Figs. 8(*b*) and 9 is localized at the fracture surface. The plastic shear displacement must therefore have been produced at high stress, just prior to fracture. This expectation was confirmed by examination of several specimens which had been unloaded prior to fracture. These exhibited only scattered clusters of straight shear steps of the sort produced by bending to large radius, Fig. 7. These steps, generally, about 0.5 mm in length, often originated at imperfections on the sample surface. They were oriented at from 90 to 45 deg with respect to the tensile axis so that they can all be accounted for as traces of the intersections with the surface of various planes of maximum shear. Finally, we note that the extent of the shear displacement shown in Fig. 9 is not uniform, but decreases gradually and becomes very small near the region where the fracture surface changes orientation. This behavior is illustrated in Fig. 9 where a transition region appears on the right-hand side of the low magnification micrographs.

DISCUSSION

The observations described above are, to our knowledge, unique, although other materials do exhibit flow and fracture behavior that is similar in some aspects. For example, steels fractured at the brittle-ductile transition[17,18] temperature often exhibit shear plane fracture surfaces and local necking ridges similar to those observed in this study. As a further example, polystyrene[19] exhibits local necking on tensile craze cracked fracture surfaces. It is noteworthy that in each of these materials, a small temperature increase produces a large change in ductility. This observation and the apparently viscous relaxation of the necked filaments at vein triple points suggest that a portion of the mechanical work expended during rupture produces local heating of the material in the necked regions.

Aside from the local necking patterns, macroscopic shear similar to that described here is commonly observed in crystalline specimens when the work-hardening rate is nearly zero, or when "adiabatic" heating of the deforming region lowers the effective hardening rate to nearly zero.[20-22] This latter phenomenon, commonly referred to as "adiabatic shear," occurs catastrophically whenever the rate of decrease in strength due to "adiabatic" heating of the deforming region equals or exceeds the rate of strengthening due to the increased strain and strain rate. If the usually small strain rate effect is neglected, the shear strength may be expressed as a function of strain and temperature:

$$\frac{d\tau}{d\gamma} = \left(\frac{\partial\tau}{\partial\gamma}\right)_T + \left(\frac{\partial\tau}{\partial\Delta T}\right)_\gamma \frac{d\Delta T}{d\gamma} \qquad [1]$$

The criterion for catastrophic shear, $d\tau/d\gamma \leq 0$, may thus be written:

$$0 \leq \frac{\left(\frac{\partial\tau}{\partial\gamma}\right)_T}{-\left(\frac{\partial\tau}{\partial\Delta T}\right)_\gamma \frac{\tau}{\alpha C}} \leq 1 \qquad [2]$$

where $\tau/\alpha C = d\Delta T/d\gamma$, C is the specific heat, τ and γ are the shear stress and strain respectively, and $\alpha \leq 1$ depending upon the degree of adiabaticity of the process.

Values for the quantities appearing in Eq. [2] may at best only be estimated. For $(\partial\tau/\partial\Delta T)_{\gamma=1\%}$ the data of Masumoto and Maddin[7] suggest a value of approximately -1.4×10^7 dyne per sq cm per deg for the region from 0° to 350°C and a much larger negative value for higher temperatures. C may be estimated

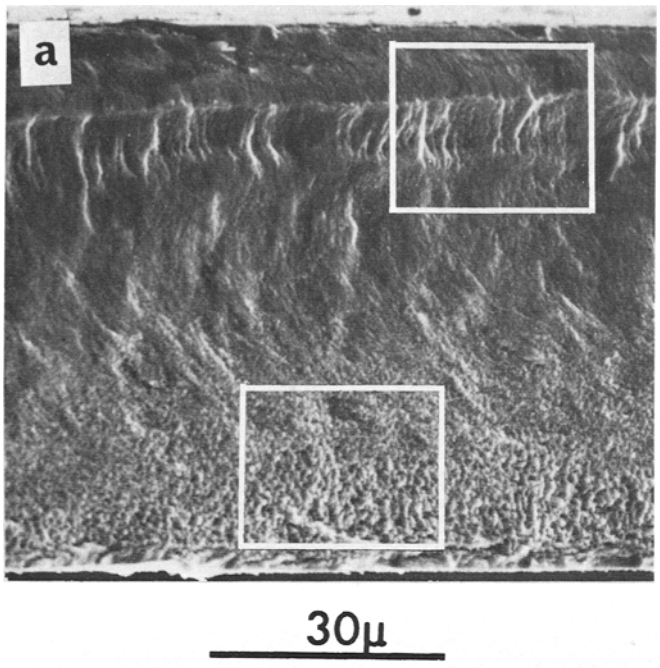

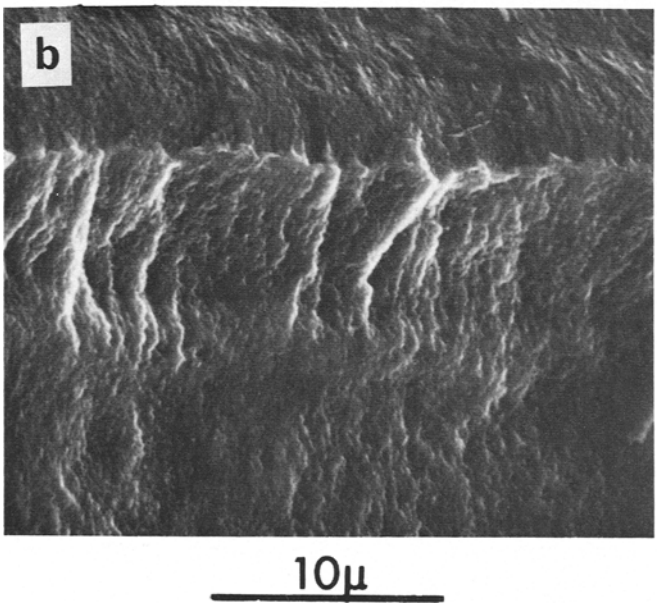

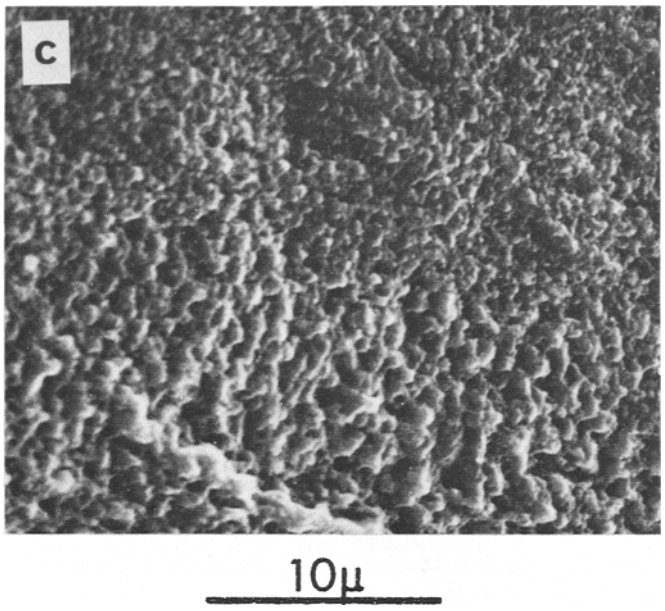

Fig. 6—The two zone fracture surface typical of a $Pd_{0.795}Au_{0.04}Si_{0.165}$ alloy which has been annealed at 450°C for 2 hr. The region of crack initiation appears at the lower edge of Fig. 6(*a*), and is shown in greater detail in Fig. 6(*c*).

as 2.5×10^7 erg per cu cm per deg, and τ is about 1×10^{10} dyne per sq cm. Insertion of these quantities into Eq. [2] leads to the prediction that $(\partial\tau/\partial\gamma)_T$ must be of the order of 5×10^9 if "adiabatic" shear is to be considered as a plausible explanation for the shear failure of these metallic glasses. From Fig. 1 a value of $(\partial\sigma/\partial\epsilon)_T$ of approximately 4×10^{11} dyne per sq cm is obtained. The conditions for catastrophic shear can therefore only be met if the "nucleating" deformation[20] is inhomogeneous to the extent that the shear occurs in bands of thickness less than about 10^{-3} cm. This possibility appears likely in view of the localized nature of the shear steps observed on unloaded specimens. In addition, the assumption of adiabatic conditions ($\alpha = 1$) seems a reasonable first approximation since the thermal diffusivity of these specimens is rather lower than that of a crystalline specimen ($\alpha \propto \kappa^{-1/2}$). Chin *et al.*[20] have shown that the fulfillment of condition [2] indicates only that adiabatic flow will occur if nucleated. The extent of the catastrophic flow depends upon the elastic energy stored in the deforming system (*i.e.* the tensile machine and specimen) and is proportional to $\sqrt{m/k}$ where m and k are the effective mass and stiffness of the elastic members. Massive loading systems* extend the duration of unstable flow but make initiation more difficult. The absence of load drops in the curves shown in Fig. 1 is therefore to be expected in view of the large amount of elastic energy stored in the specimen. Finally, we note that the "degree of adiabaticity," α, is proportional to the strain rate.[22] That is, the stress at which catastrophic flow occurs will decrease with increasing strain rate. This relationship has been reported by Masumoto and Maddin[7] for the fracture stress of an amorphous $Pd_{0.8}Si_{0.2}$ alloy.

*An Instron model TM testing machine was used in this study

During localized shear deformation, tensile specimens are restrained by the grips and cannot undergo free lateral displacement as depicted in Fig. 8. The specimens are therefore subjected to a bending moment which increases with shear strain. For single crystal specimens this moment produces plastic deformation near the grips, but does not affect the slip system, which is determined by the crystal structure. In the amorphous specimens tested here, shear deformation is not constrained to a particular direction. At any given elongation, the lateral displacement is resisted by a force proportional to the moment of inertia of the specimen cross-section; *i.e.* proportional to the square of the specimen thickness measured in the direction of lateral displacement. This resistance is smallest for a shear direction in the plane perpendicular to the broad face of a ribbon specimen and evidently explains the consistent observation of shear failure in this direction.

The experimental observation of shear deformation below the fracture stress leads via well-established

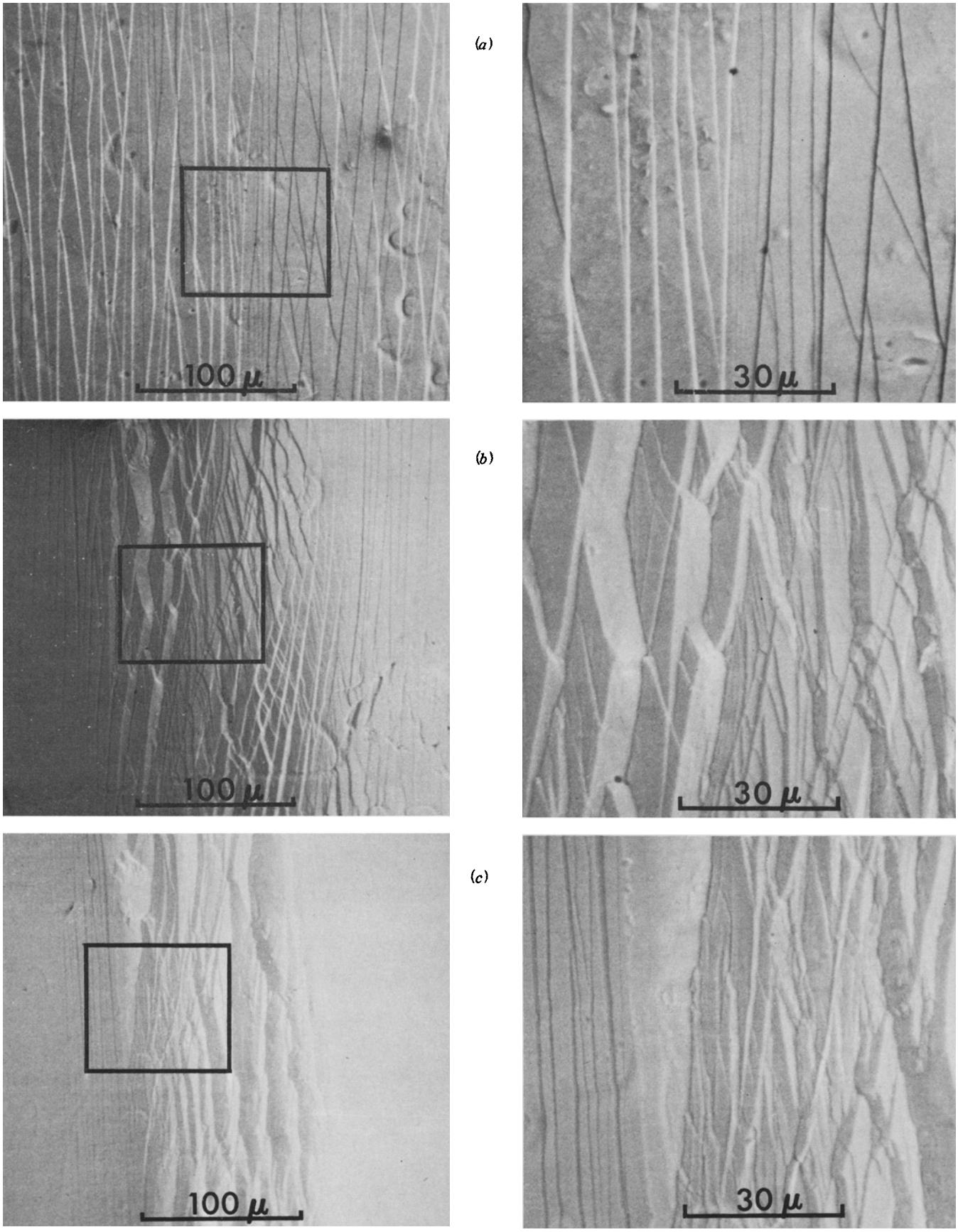

Fig. 7—Deformation markings produced by bending an amorphous $Pd_{0.82}Si_{0.18}$ alloy. The deformation markings shown in Figs. 7(*a*), 7(*b*), and 7(*c*) were produced by bending the outermost specimen surface to a radius of 405, 145, and 75 μ respectively. The outlined areas are shown at higher magnification in the right-hand micrograph of each pair, and the bend axis is oriented vertically.

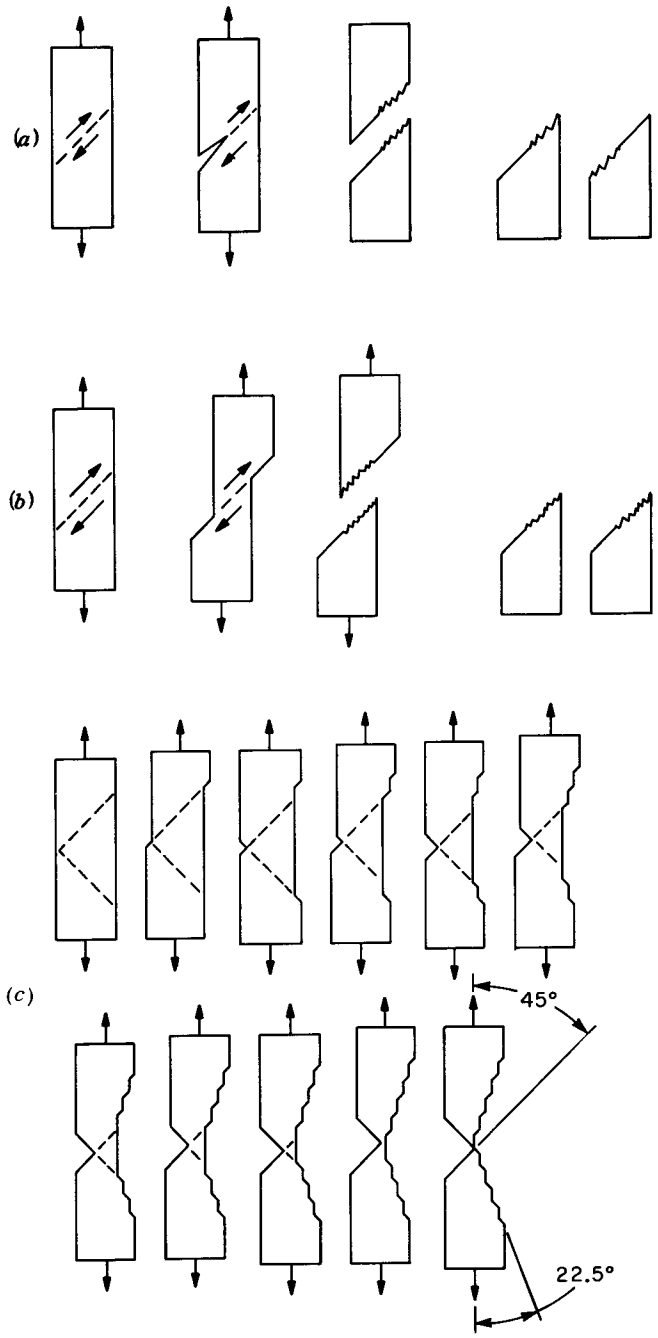

Fig. 8—Schematic illustration of possible shear fracture modes in ribbon specimens. (*a*) Shear crack propagation; (*b*) Plastic shear and fracture; (*c*) Alternating shear.

arguments[23] to the question: Is the deformation in the shear surface homogeneous or do some areas deform before others? This question may be considered by estimating the stress required for homogeneous shear of an amorphous alloy. Following Frankel's classical argument for the crystalline case, the energy of a defect-free close-packed crystal which is sheared an amount x/d on a close-packed plane is represented by $-A \cos 2\pi(x/d)$, where d is the interatomic spacing. It is easily shown that the stress required for homogeneous shear is $\mu/2\pi$.[23] Refinements in the assumed energy-displacement curve reduce the theoretical shear stress to about 0.03 μ. For amorphous and microcrystalline materials, the first neighbor distance is little different than that of the crystal but long range periodicity is not present. The potential energy of a rigidly sheared amorphous material will therefore be determined by the local atomic configurations which, during shear, produce the largest displacement perpendicular to the shear surface. We therefore expect that the energy change accompanying a rigid shear displacement across the weakest surface in any given direction will rise to a value higher than that encountered in crystals and remain at this level as x/d is increased. Once initiated, only the stress required to create the new surface is needed to maintain the displacement and rigid shearing should proceed to fracture.

Alternatively, if relaxation of the atoms in the neighborhood of the sheared surface is allowed, the energy increase accompanying shear is decreased and the energy vs x/d relation may possess minima. The existence of such minima changes the deformation process fundamentally. That is, parts of the material will have undergone permanent shear deformation and relaxed to near equilibrium glassy or crystalline configurations while other regions will have relaxed into positions only slightly different from their original locations. In this case the dislocation-like boundaries which separate the sheared from unsheared areas of the shear plane act to localize the deformation and their mobility will determine the course of deformation in the material.

Finally, if the elimination of all of the increase in energy with deformation were achieved through complete relaxation of all atoms in the stressed volume, a viscous, zero hardening rate, shear deformation would result. Note that the three deformation modes described here differ primarily in that each requires that a different degree of atomic relaxation occur during deformation. Each mode thus will occur in a different range of temperature and strain rate. Although the stresses involved are difficult to estimate, the experimental data described here suggests that amorphous $Pd_{0.8}Si_{0.2}$ alloys deform via motion of localized strain concentrations at room temperature.

Examination of the tensile deformation and fracture behavior of several amorphous and microcrystalline alloys has shown that:

a) Tensile stress is accommodated by high hardening rate plastic shear deformation;

b) Fracture occurs on surfaces of maximum shear stress and is preceded by plastic shear strain of as much as 40 pct.

c) Fracture is accompanied by local heating and viscous flow necking of material between propagating cracks or voids.

These observations form the basis for speculation that plastic flow occurs via motion of localized strain concentrations and that fracture is initiated by macroscopic "adiabatic" shear.

ACKNOWLEDGMENTS

We acknowledge with gratitude helpful discussions with G. Y. Chin, P. L. Key, J. C. M. Li, J. R. Low, Jr., and D. R. Uhlmann. The portion of the work performed at Yeshiva University was carried out under Contract No. AFOSR 69-1642 and NR-N00014-69-A-0411.

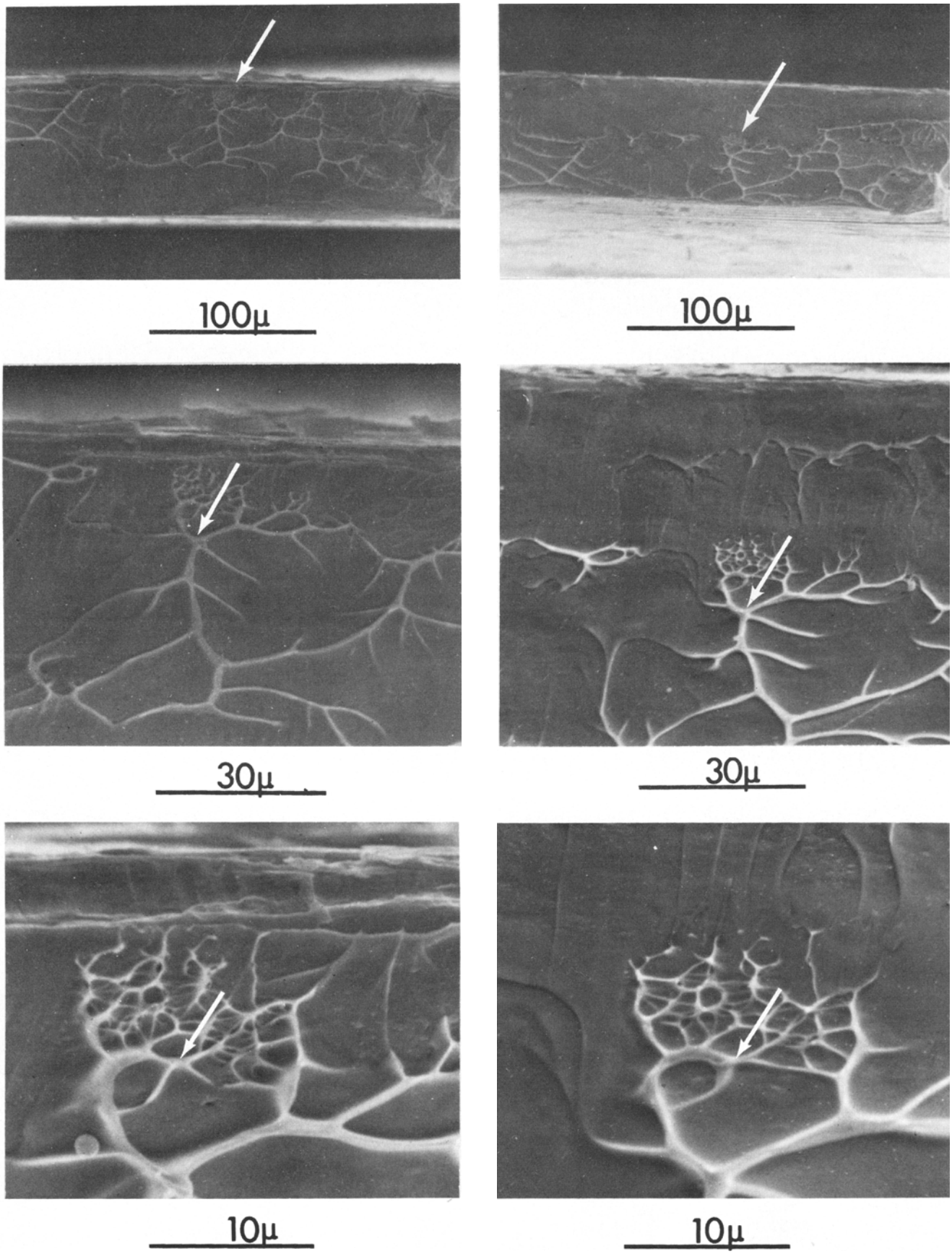

Fig. 9—The fracture morphology of opposing segments of an amorphous $Pd_{0.82}Si_{0.18}$ alloy (tensile specimen No. 1). The micrographs in the left column were printed with the negative reversed to facilitate comparison with those from the opposite surface, shown in the right-hand column. White arrows mark corresponding points on the two surfaces.

REFERENCES

1. W. Klement, R. H. Willens, and P. Duwez: *Nature (London),* 1960, vol. 187, p. 869.
2. H. S. Chen and D. Turnbull: *Acta Met.,* 1969, vol. 17, p. 1021.
3. H. S. Chen: unpublished research, Allied Chemical Corporation Research Laboratories, Morristown, N. J., 1970.
4. P. Duwez: *Trans. ASM,* 1967, vol. 60, p. 605.
5. H. S. Chen and T. T. Wang: *J. Appl. Phys.,* 1970, vol. 41, p. 5338.
6. H. S. Chen, H. J. Leamy, and M. Barmatz: *J Noncryst. Solids,* 1971, vol. 5, p. 444.
7. T. Masumoto and R. Maddin: *Acta Met.,* 1971, vol. 19, p. 725.
8. G. S. Cargill: *J. Appl. Phys.,* 1970, vol. 41, pp. 12 and 2248.
9. J. D. Bernal: in *Liquids: Structure, Properties, and Solid Interactions,* T. J. Hughel, ed., p. 25, Elsevier Publishing Company, Amsterdam, 1965.
10. H. S. Chen and C. E. Miller: *Rev. Sci. Instrum.,* 1970, vol. 41, p. 1237.
11. M. F. Ashby, A. N. Nelson, and R. M. A. Centamore: *Scripta Met.,* 1970, vol. 4, p. 715.
12. D. Weaire, M. F. Ashby, J. Logan, and M. J. Weins: *Acta Met.,* 1971, vol. 19, p. 779.
13. D. M. Marsh: *Proc. Roy. Soc., London,* 1964, vol. A279, p. 420.
14. J. D. Mackenzie and R. P. LaForce: *Nature, London,* 1963, vol. 197, p. 480.
15. J. R. Low, Jr.: in *Fracture of Solids,* D. C. Drucker and J. J. Gilman, eds., pp. 197-236, Interscience Publishers, New York, 1963.
16. R. M. N. Pelloux: *Eng. Fracture Mech.,* 1970, vol. 1, p. 697.
17. C. Crussard, J. Plateau, R. Tamhankar, G. Henry, and D. Lajeunesse. in *Fracture,* B. L. Averbach, D. K. Felbeck, G. T. Hahn, and D. A. Thomas, eds., p. 52.1, John Wiley and Sons, Inc., New York, 1959.
18. C. D. Beachem and R. M. N. Pelloux: *Amer. Soc. Test Mater., Spec. Tech. Publ.,* 1964, No. 381, pp. 210, 245.
19. J. Murray and D. Hull: *J. Polymer Sci.,* 1970, vol. 8, part A-2, p. 583.
20. Z. S. Basinski: *Proc Roy. Soc., London, Ser. A,* 1957, vol. 240, p. 229.
21. G. Y. Chin, W. F. Hosford, Jr., and W. A. Backofen: *Trans. TMS-AIME,* 1964, vol. 230, p. 1043.
22. R. F. Recht: *J. Appl. Mech.,* 1964, vol. 31, p. 189.
23. A. H. Cottrell: *Dislocations and Plastic Flow in Crystals,* Oxford University Press, London, 1953.